2020 IEEE/RSJ International Conference on Intelligent Robots and Systems (IROS)
October 25-29, 2020, Las Vegas, NV, USA (Virtual)

Operational Space Formulation and Inverse Kinematics for an Arm Exoskeleton with Scapula Rotation

Craig Carignan[1], Daniil Gribok[2], Tuvia Rappaport[3], and Natalie Condzal[4]

***Abstract*— The operational space of an 8-axis arm exoskeleton is partitioned into "tasks" based on the human arm motion, and a task priority approach is implemented to perform the inverse kinematics. The tasks are prioritized in the event that singularities or other constraints such as joint limits render the full desired operational space infeasible. The task reconstruction method is used to circumvent singularities in a deterministic manner so that the arm is never physically in a singular configuration. This is especially advantageous when the arm is fully extended because it allows the hand to move smoothly along the workspace boundary. The task priority inverse kinematics approach is also more computationally efficient than full Jacobian inverse methods and naturally manages the motion of the arm in a more anthropomorphic-friendly manner. The new methodology is demonstrated with four operational tasks on the MGA Exoskeleton.**

I. INTRODUCTION

Exoskeletons have a larger operational space than manipulators since they encompass and must therefore follow the motion of the whole arm. The human arm is considered to have seven gross degrees of freedom (DOF) – three for the shoulder, one for the elbow, and three for the wrist [10] – but in reality, there are many more. For example, the shoulder is not simply a 3-DOF ball and socket joint but realizes translation as well due to the scapula-humeral complex [19]. In fact, passive spring-loaded degrees of freedom have been incorporated to accommodate additional movements of the human arm inside the exoskeleton to make the more ergonomic [27]. The MGA Exoskeleton (MGAXOS) shown in Fig. 1 uses a single DOF for shoulder elevation and depression in addition to 7 DOF for the basic arm motion.

Exoskeletons therefore require an "augmented" Jacobian approach to map the joint space to the operational space [21]. The task priority inverse kinematics (TPIK) approach [25] is an effective method for resolving the inverse kinematics of higher dimensional workspaces. In this approach, the inverse kinematics can be partitioned into tasks, which can be prioritized so that the most important task is achieved first. Thus if the desired trajectory cannot be achieved due to encountering a singularity, then the lower priority task is modified in order to avoid the occurrence of singularities. While task-priority inverse kinematics is typically applied to hyper-redundant kinematic structures, such as snake robots or anthropomorphic kinematic chains [2], it also offers significant computational advantages because of the lower dimensionality of the subtasks.

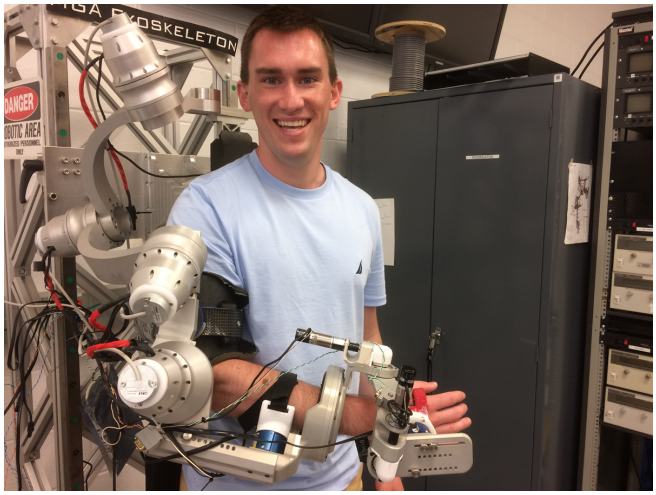

Fig. 1. The MGA Exoskeleton has eight rotary joints and four adjustable sliding linkages.

While this strategy addresses the kinematic redundancy with respect to the hand motion, the augmented Jacobian introduces "algorithmic" singularities in the joint space. A singularity is the result of two or more joint motions becoming linearly dependent with respect to the operational space, which causes the rank of the Jacobian to collapse. Kinematic singularities result from the linear dependence of the Jacobian mapping between the end-effector and joint space, and their locations can usually be analytically determined for 6-DOF arms and even some 7-DOF arms [20]. Algorithmic singularities result from the additional task variables and occur even when the end-effector Jacobian is full rank [7]. The location of algorithmic singularities are usually difficult (if not impossible) to determine analytically, necessitating a singularity avoidance approach that does not rely on a priori knowledge of their locations.

A common singularity handling technique is the "Damped Least Squares" (DLS) method which adds a small damping factor to the singular values of the Jacobian when it becomes singular [3], [26]. This approach sometimes incorporates a weighting matrix for the Jacobian that de-emphasizes

[1]C. Carignan is an adjunct professor with the Dept. of Aerospace Engineering, University of Maryland, College Park, Maryland 20742 USA craigc@ssl.umd.edu

[2]Daniil Gribok is a graduate research assistant with the Department of Aerospace Engineering, University of Maryland, College Park, Maryland 20742 USA dgribok@ssl.umd.edu

[3]Tuvia Rappaport is an undergraduate research assistant with the Department of Aerospace Engineering, University of Maryland, College Park, Maryland 20742 USA tcrappa@terpmail.umd.edu

[4]Natalie Condzal is an undergraduate research assistant with the Department of Aerospace Engineering, University of Maryland, College Park, Maryland 20742 USA ncondzal@terpmail.umd.edu

directions in which it cannot move [8] or takes into account inertial parameters for smoothing the dynamics near singularities [6]. However, the DLS method has the undesirable side-effect of producing unpredictable motion through the distortion of the inverse Jacobian mapping from Cartesian to joint space, which may be disconcerting to the operator.

Another approach is to circumvent the singularity altogether via a process called "task reconstruction" [18]. In this method, a boundary is defined around a singularity measure that goes to zero at the singularity, and the path in the task space is modified so that it never penetrates this boundary. While the "reconstructed" path will deviate from the desired path, it travels predictably along the singularity boundary until it no longer violates the manipulability constraint and then merges back with the original path. In addition to producing a singularity-free path, the methodology is easily extensible to multiple tasks within the operational space.

The main contribution of this work is the decomposition of the operational space of more complex exoskeleton designs into "anatomical" subspaces enabling task-prioritized inverse kinematics to be applied. The decomposition also produces decoupling of the singularity conditions so that the locations and consequences of the singularities can be determined. Moreover, the application of the task reconstruction method to singularity avoidance produces smooth behavior at the workspace boundary. The article begins with an overview of the exoskeleton kinematics in Section II. The operational space for the exoskeleton is developed in Section III and a summary of the singularity analysis is given in Section IV. The task priority inverse kinematics for the exoskeleton are developed in Section V, and singularity avoidance is described in Section VI. Simulation results are presented in Section VII and conclusions in Section VIII.

II. KINEMATIC MODEL

The schematic in Fig. 2 illustrates the articulation of the MGA Exoskeleton [13]. The scapula joint 1 located at B rotates the shoulder S along an arc of radius $\overline{BS}$. Joints 2-4 enables 3-axis rotation about the shoulder gleno-humeral (GH) joint located at S. Joint 5 generates elbow flexion/extension. The supination/pronation joint 6 produces forearm rotation about line $\overline{EW}$. The wrist joints 7 and 8 produce flexion/extension and abduction/adduction, respectively. There is an offset of $L_w = 5$ mm between the wrist joints which causes movement along an ellipsoidal surface [1]. The scapula, upper arm, forearm, and hand links contain passive prismatic joints to accommodate variable subject geometry with ranges $L_s = 13.6 - 21.2$ cm, $L_u = 30.4 - 36.0$ cm, $L_f = 23.7 - 33.3$ cm, and $L_h = 4.3 - 9.7$ cm. The fixed lengths are $L_1 = 17.36$ cm and $L_2 = 16.12$ cm.

The link frame diagram for the MGA Exoskeleton in Modified Denavit-Hartenberg (D-H) Notation is shown in Fig. 3, and the D-H parameters are given in Table I [9]. The leading "scapula" joint is mounted perpendicularly to the back roughly above the human sternoclavicular (SC) joint and is used to approximate shoulder elevation and depression [24]. (It is not a redundant joint for shoulder rotation [15].)

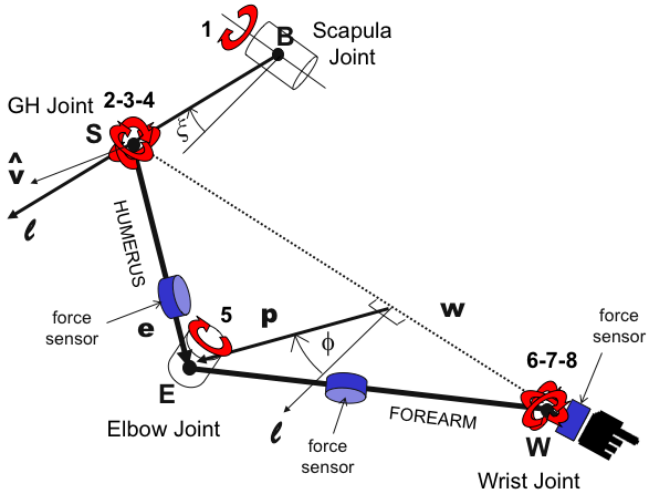

Fig. 2. Schematic representation of MGAXOS showing four anatomical joint groups and locations of force sensors.

An orthogonal, intersecting-axis triad is used to generate the 3-axis rotation about the shoulder. The first shoulder axis is mounted at a $30°$ angle from vertical to rotate the gimbal lock singularity away from the vertical position (alignment of axes 2 & 4) [14]. The third shoulder axis intersects the upper arm link at an angle of $45°$ (rather than being coincident) to increase the range of motion [22]. A pitch joint

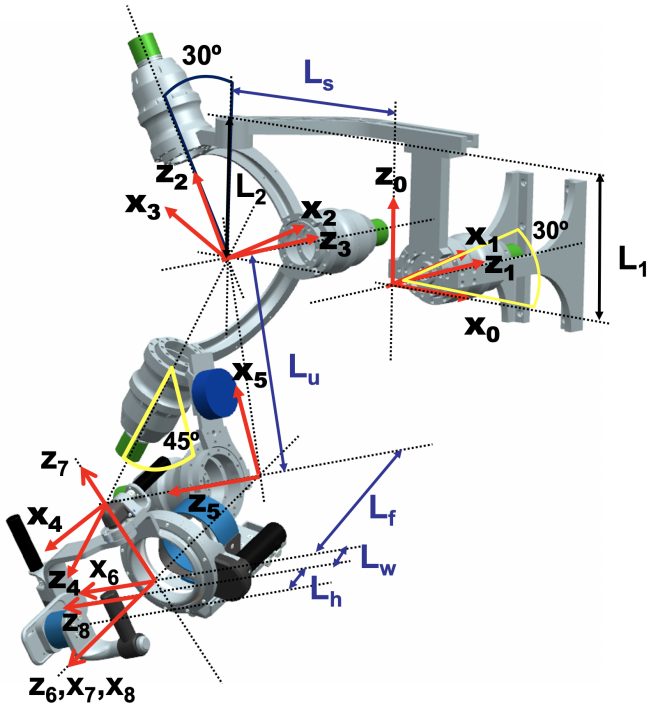

Fig. 3. D-H link frame diagram of MGA Exoskeleton with eight actuated revolute joints and four passively adjustable linkages (L_h, L_f, L_u, L_s).

drives elbow flexion/extension with a hardstop to prevent extension beyond $0°$. The elbow is connected to the wrist via a forearm link with a passive sliding adjustment and

a pronation/supination joint driven by a motor mounted at the distal end of the link. The wrist flexion/extension and abduction/adduction joints are then placed orthogonally to each other with an axis offset of L_w. The handle is then attached to the abduction/adduction link which has a passive adjustment of L_h along the x-axis to accommodate different wrist-to-palm distances.

TABLE I
MODIFIED D-H PARAMETERS FOR MGAXOS†

link i	α_{i-1} (deg)	a_{i-1} (cm)	d_i (cm)	θ_i* home (deg)
1	-90	0	0	-30
2	$+90$	$-L_{sg}\cos(30^\circ+\beta)$	$L_{sg}\sin(30^\circ+\beta)$	0
3	-90	0	0	-105
4	$+90$	0	$L_u/\cos(45^\circ)$	-90
5	-45	0	$-L_u$	0
6	$+90$	0	L_f	90
7	$+90$	0	0	90
8	$+90$	L_w	0	0

† $L_{sg}=\sqrt{L_s^2+(L_1-L_2)^2}$ and $\beta=\arccos(L_s/L_{sg})$

III. OPERATIONAL SPACE FORMULATION

The operational space for the exoskeleton is divided into the four tasks shown in Table II. The scapula elevation is chosen as Task 1 because it depends on the desired arm elevation, so it is essentially a dependent variable [24]. It is not desirable to use it for controlling hand pose or the self-motion angle. By giving the scapula elevation first priority, it will always be achievable unless a kinematic constraint overrides it. The hand position and orientation are the next priority tasks. Position is chosen for Task 2 since it is generally more important than orientation, but the order of these priorities can be swapped depending upon the goal.

The "self-motion" angle of the arm is chosen for Task 4. Self-motion is defined as any motion of the joints that does not cause a change in the pose of the handle. One measure of the self-motion is the angle that the plane connecting the shoulder, elbow, and wrist (SEW) joints makes about the shoulder-wrist vector, w, with respect to some reference plane as shown in Fig. 2 [21]. In biomechanics, this angle is referred to as the "swivel" angle, and the reference plane is the vertical plane passing through the shoulder and the wrist [16]. Self-motion can be controlled independently of the hand for obstacle avoidance or mechanical advantage.

TABLE II
OPERATIONAL SPACE TASK PRIORITIZATION FOR EXOSKELETON

order	task	symbol	DOF
1	scapula elevation	ξ	1
2	handle position	p_h	3
3	handle rotation	R_h	3
4	SEW angle	ϕ	1

In order to develop a motion control strategy, the Jacobians relating the four task velocities to the joint rates need to be determined.

A. Scapula Jacobian

Since scapula elevation is simply the joint 1 angle, $\xi=\theta_1$, the scapula Jacobian $J_\xi \equiv \frac{\partial \xi}{\partial q}$ is trivially given by

$$J_\xi = [\,1\;\;0\;\;0\;\;0\;\;0\;\;0\;\;0\;\;0\,] \tag{1}$$

where q is the 8×1 vector of joint angles, θ_i.

B. Handle Jacobians

The homogenous local link transforms from the base frame to the last link frame can be multiplied to find the link axis projections z and relative handle positions p_h used below [9]. The rotation Jacobian in link frame i is then the 3×8 matrix whose columns are the projections of the link axis unit vectors onto frame i:

$${}^iJ_r = \left[{}^iz_1 \mid {}^iz_2 \mid \cdots \mid {}^iz_8\right] \tag{2}$$

The translation Jacobian in link frame i is also a 3×8 matrix and can be found via direct differentiation of the handle position, $J_t \equiv \frac{\partial p_h}{\partial q}$, or the cross-product method [28]

$${}^iJ_t = \left[{}^iz_1\times{}^i({}^1p_h) \mid {}^iz_2\times{}^i({}^2p_h) \mid \cdots \mid {}^iz_8\times{}^i({}^8p_h)\right] \tag{3}$$

where ${}^i({}^jp_h)$ is the position of the handle with respect to frame j in frame i.

C. SEW Jacobian

Define w and e as the vectors from the shoulder to the wrist and elbow, respectively, and let $\hat{v}$ denote an arbitrary fixed unit reference vector in frame 0. The SEW angle, ϕ, is then defined as the angle between p and ℓ

$$\tan\phi \equiv \frac{\hat{w}^T(\ell\times p)}{\ell^T p} \tag{4}$$

The SEW angle is calculated by using the forward kinematics to compute w and e and then performing the vector operation in (4) numerically.

The Jacobian of the SEW angle, $J_\phi \equiv \frac{\partial \phi}{\partial q}$, is then found from

$$\begin{aligned} J_\phi \;=\; & \frac{(\hat{w}\times\hat{p})^T}{||p||}E \\ & + \left\{\frac{\hat{v}^Tw}{||\ell||}(\hat{w}\times\hat{\ell})^T - \frac{\hat{w}^Te}{||w||||p||}(\hat{w}\times\hat{p})^T\right\}W \end{aligned} \tag{5}$$

where $E\equiv\frac{\partial p_e}{\partial q}$ and $W\equiv\frac{\partial p_w}{\partial q}$ are the Jacobians of the elbow and wrist positions, respectively, which are computed similarly to the handle translation Jacobian [21]. Because the SEW angle is only a function of θ_1 to θ_5, the last three elements of the 1×8 matrix J_ϕ are zero.

IV. SINGULARITIES

The singularities of the exoskeleton occur when the determinant of the 8×8 Jacobian relating the four task velocities to the joint velocities is zero. However, since the scapula rotation is the highest priority task and is always satisfied by joint 1, Task 1 is never singular. Moreover, since the first joint only orients the exoskeleton with respect to inertial space, singularities are never a function of the first joint

angle. Therefore, the first column and row of the augmented Jacobian can be dropped from the singularity analysis. This leaves the following 7×7 Jacobian to be analyzed for singularities of the handle pose and self-motion angle:

$$J = \begin{bmatrix} J_t^1 \\ J_r^1 \\ J_\phi^1 \end{bmatrix} \tag{6}$$

where J^j represents J with the j^{th} column deleted.

The "kinematic" singularities occur when the rank of the "tool" Jacobian (J with J_ϕ^1 deleted) falls below 6. Assuming a three-axis intersecting wrist ($L_w = 0$) permits a significant simplification since the singularities of tool Jacobian are the same as the "wrist" Jacobian found by setting $L_h = 0$ in the tool Jacobian [20]:

$$J_w = \begin{bmatrix} J_{11} & 0 \\ J_{21} & J_{22} \end{bmatrix} \tag{7}$$

where $J_{11}, J_{21} \in \mathbb{R}^{3\times4}$ and $J_{22} \in \mathbb{R}^{3\times3}$ are partitions of the wrist Jacobian, and 0 is a 3×3 matrix of 0's. Using the Cauchy-Binet Formula [11], the determinant of $J_w J_w^\mathsf{T}$ can be transformed into a sum of determinants from which the singularity conditions can be derived (see Appendix).

The resulting analysis reduces to the four singularity types shown in Table III. At least one condition involves the alignment of a pair of joint axes. Type 1 is a workspace boundary singularity caused by an elbow pitch of $0°$, which causes full extension of the arm. Types $2-4$ represent internal workspace singularities. Types 2 and 3 require alignment of the first and third shoulder axes so that $\sin(\theta_3) = 0$. Correspondingly, $\theta_3 = -180°$ is infeasible since it places the upper arm inside the torso, and $\theta_3 = 0°$ is infeasible since it causes a shoulder joint collision. Types 3 and 4 require a wrist flexion/extension of $90°$ or $\theta_7 = 0°, 180°$, which are at wrist joint hardstops and near anatomical limits.

TABLE III
KINEMATIC SINGULARITIES OF THE MGA EXOSKELETON†

Type	Condition A	Condition B
1	$s_5 = 0$	-
2	$s_3 = 0$	$\sqrt{2}(L_u/L_f + c_5)s_4 + 2c_4 s_5 = 0$
3	$s_3 = 0$	$s_7 = 0$
4	$s_7 = 0$	$c_6 = 0$

† $c_i \equiv \cos(\theta_i), s_i \equiv \sin(\theta_i)$

Although the internal singularities are physically unreachable, it is still possible to get close. Fig. 4 shows a pair of "near" singular configurations corresponding to Types 2 and 3. In addition to shoulder axis alignment, Type 2 also requires Condition B, which is a complex function of θ_4 and θ_5 due to the $45°$ angle between the third shoulder joint axis and the elbow pitch axis. The solutions are where the surface elevation in Fig. 5 is zero. [It is interesting to note that for $90°$ between joint axes 4 and 5, the condition is simply $\theta_4 = \pm 90°$.] The near Type 3 singularity shown actually corresponds to simultaneous gimbal lock in the shoulder and wrist caused by axial alignment.

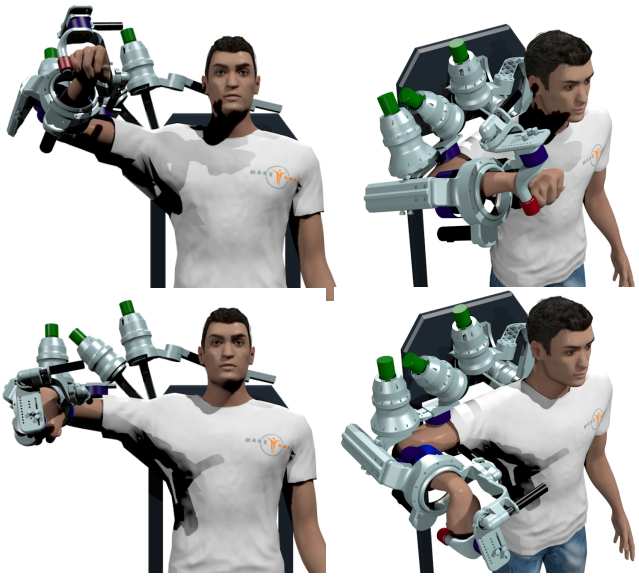

Fig. 4. Close alignment of first and third shoulder axes causes near singular conditions, Type 2 (top) $q = [-17°, 0°, -15°, -58.8°, 90°, 90°, 90°, 0°]$ and Type 3 (bottom) $q = [-17°, 0°, -15°, -90°, 90°, 90°, 165°, 0°]$.

For a 7-DOF anthropomorphic arm, the "algorithmic" singularities corresponding to self-motion occur for shoulder or wrist gimbal lock ($s_3 = 0$ or $s_7 = 0$) [21]. which are not in the anatomically reachable part of the workspace. While a zero elbow pitch ($s_5 = 0$) is technically not a singularity, the SEW angle is undefined and self-motion is simply a rotation about the should-wrist vector. In summary, the shoulder and wrist gimbal lock that cause internal singularities are effectively prevented in the anatomical region of the exoskeleton's workspace by skewing the first shoulder joint axis from the vertical and designing the wrist axes to be mutually orthogonal in the nominal hand configuration.

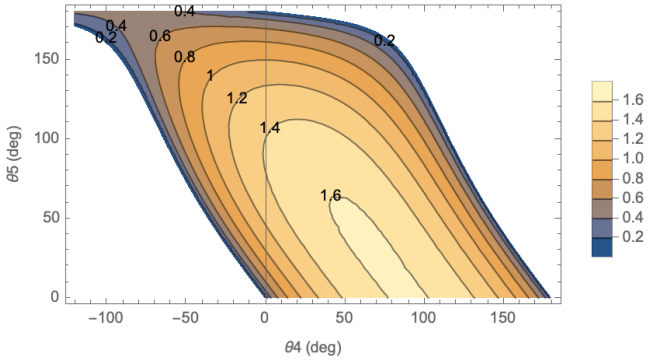

Fig. 5. Shoulder pitch/rotation singularities occur where surface Δ intersects the zero plane ($\Delta \equiv \sqrt{2}(L_u/L_f + c_5)s_4 + 2c_4 s_5$)

V. TASK PRIORITY INVERSE KINEMATICS

The motion controller is responsible for transforming operational space velocity commands, $\dot{x}$, into joint velocities, $\dot{q}$, to be sent to the joint servo controller [4], [12]. Classical approaches implementing a singularity-robust inverse [26] or damped least-squares are typically used to invert the Jacobian

matrix formed by stacking up the task space Jacobians developed in Section III [29]. The main disadvantage of these approaches is indeterministic tracking error in the vicinity of singularities.

Alternatively, the inverse kinematics can be partitioned into tasks, which can be prioritized in the event a singularity is encountered. Thus, the path for the lower priority task is modified to prevent a singularity in the higher order task. The task priority approach uses a secondary task correction and a successive task projection in order to keep the manipulability index over a predefined threshold. This implicit singularity avoidance approach is equivalent to dynamically reordering the task priority so that the manipulability constraint becomes the highest priority task when it is active [17].

In the TPIK approach [25], the task space, x, is divided into subspaces, x_i, ranked in the i^{th} order of importance. The relationship between the joint velocities $\dot{q} \in \mathbb{R}^n$ and the task space velocities $\dot{x}_i \in \mathbb{R}^{m_i}$ is given by

$$\dot{x}_i = J_i(q)\,\dot{q} \tag{8}$$

where $J_i(q) \in \mathbb{R}^{m_i \times n}$ is the Jacobian of the manipulation variable, x_i. The prioritized task decomposition leads to the following recursive formulation [23]

$$\left.\begin{array}{l} \dot{q}_i = \dot{q}_{i-1} + \hat{J}_i^{\dagger}\left(\dot{x}_i - J_i \dot{q}_{i-1}\right) \\ \hat{J}_i = J_i J_i{}^{n} \\ J_i{}^{n} = J_{i-1}{}^{n} - \hat{J}_{i-1}^{\dagger}\hat{J}_{i-1} \end{array}\right\} \begin{array}{l} \dot{q}_0 = 0 \\ J_0 = 0 \\ J_0{}^{n} = I_n \end{array} \tag{9}$$

where $J_i^{\dagger}(q) \in \mathbb{R}^{n \times m_i}$ is the right pseudoinverse of $J_i(q)$.

The task decomposition process is illustrated in Fig. 6 for four tasks. The operational space path x enters from the left and gets differenced with the previous position along the path. The change, δx, is then decomposed into the desired change for Task 1, δx_1. The Jacobian pseudoinverse for Task 1 is then used to find the minimum norm solution, δq_1, that will achieve Task 1. If that causes a constraint violation, then a task reconstruction process is invoked to change δx_1 so that the constraint is satisfied. This process continues through Task 4, and then all of the changes δq_i are summed together to produce the total change in the joint angles, δq.

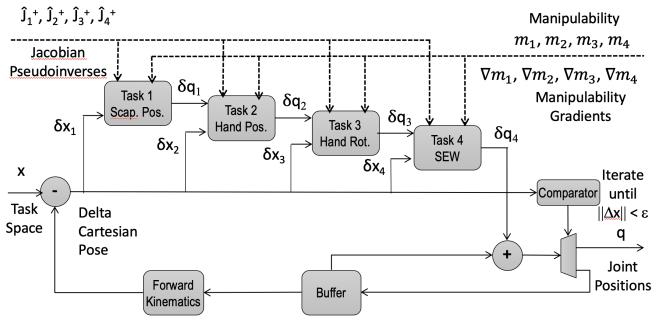

Fig. 6. Task priority decomposition procedure for four tasks.

VI. Singularity Avoidance

The task decomposition process breaks down when a task Jacobian in (9) is not invertible. In the vicinity of a singularity, the task reconstruction method is applied to circumvent the singular configuration. The manipulability index, $m(q)$,

$$m(q) = \sqrt{\det\left[JJ^T\right]} \tag{10}$$

is a continuous non-negative scalar that becomes equal to zero only when the Jacobian matrix is not full rank [30]. Since m is exactly the product of the singular values of J, it can be regarded as a distance from singularity [23]. If any singular value is 0, then the manipulability index is zero.

A small variation of $m(q)$ is given by:

$$\delta m(q) = \frac{\partial m(q)}{\partial q}\delta q = \frac{\partial m(q)}{\partial q} J^{\dagger}\delta x \tag{11}$$

In order for $\pm\delta m(q) = 0$, (11) implies that the given task change must be orthogonal to the vector, $\frac{\partial m(q)}{\partial q}J^{\dagger}$, or, equivalently, that $\pm\delta x$ must lie on the surface defined by:

$$\left(\frac{\partial m(q)}{\partial q}J^{\dagger}\right)\cdot \delta x = 0 \tag{12}$$

where $x \in \mathbb{R}^m$. If the quantity in parentheses in (12) is the surface normal, n_m, then the projection of the given task on the singularity surface is given by:

$$\delta x_p = \delta x - (\delta x \cdot n_m)n_m = (I_m - n_m n_m^T)\delta x \tag{13}$$

Thus δx_p represents the task change that avoids the singularity. Fig. 7 illustrates the reconstructed path as it intersects and then moves along the singularity surface $m = \overline{m}$.

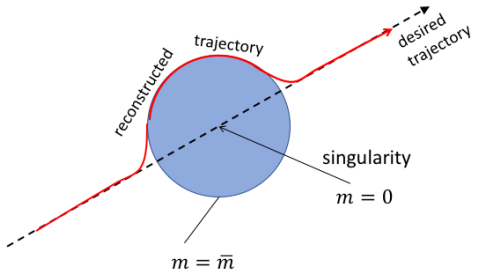

Fig. 7. Task reconstruction is used to circumvent a singularity.

VII. Simulations

A block diagram of the exoskeleton motion control system architecture is shown in Fig. 8. Input task commands, δx, are issued by hand controllers or a graphical interface on the Command Computer. The trajectory generator in the Control Computer then sends the task space commands to the TPIK velocity solver which determines the change in joint angles. The joint angle changes are converted to rates and then streamed to the exoskeleton velocity servo controller. In addition, the task commands are integrated and an error loop is formed with the forward kinematics of the integrated joint velocity output to correct for drift.

The task-priority inverse kinematics was demonstrated with the visualization tool on the exoskeleton simulator. The joint angle commands are also streamed to a Unity visualization used to create virtual environments viewed by

the operator through an Oculus Rift headset. Simulations ran at a loop rate of 100 Hz, and the task position error loop gain was set to 10. The link lengths were set to: $L_s = 20$ cm, $L_u = 30$ cm, $L_f = 35$ cm, and $L_h = 5$ cm.

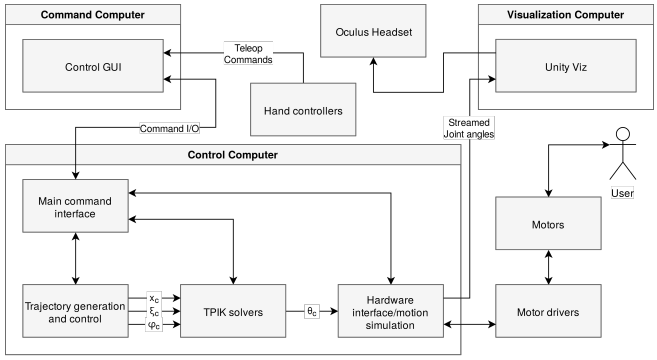

Fig. 8. Exoskeleton motion controller architecture.

A. Trajectory into Workspace Boundary

The handle was commanded to move at 1 cm/s in the forward ($-y_0$ direction) starting from $p_h^T = [-0.2\ 0.4\ 0]$ m while the handle axes stayed aligned with the base frame axes. The SEW angle and scapula angles where held fixed at $\phi = 0°$ and $\xi = -30°$. The value of the manipulability and transition boundaries was set to 0.02 for all four tasks.

The plot of the handle position shows pure translation in the y-direction in Fig. 9 until the singularity avoidance takes effect for Task 2. The plot of manipulability for Tasks 2-4 are shown in Fig. 10. As the arm extends toward the workspace boundary, the handle translation manipulability m_2 is seen to decrease until it reaches the manipulability boundary at $\overline{m} = 0.02$. The path is then reconstructed so that it travels along the singularity boundary so that the position of the handle is never commanded past the workspace boundary.

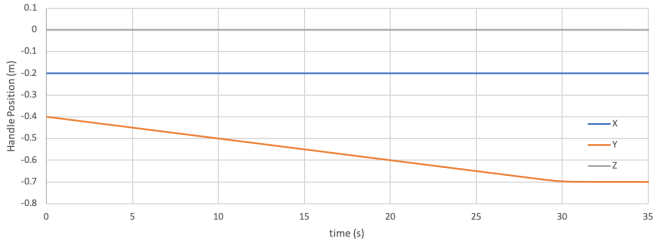

Fig. 9. Position of handle during move into workspace boundary.

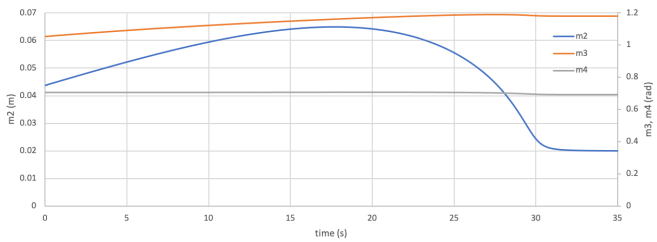

Fig. 10. Manipulability indices during move into workspace boundary.

B. Trajectory Passing Near Internal Singularity

The handle is commanded to move vertically from -20 cm below the near singular pose shown at the top of Fig. 4 to 10 cm above it. The SEW angle was fixed at $\phi = -92.0°$, and the commanded scapula angle ξ was calculated based on the elevation angle of the upper arm so as to maintain proper scapulohumeral rhythm of the shoulder [5]. The manipulability bounds were set to $\overline{m}_2 = 0.02$, $\overline{m}_3 = 0.4$, and $\overline{m}_4 = 0.02$, and the transition bounds were set equal to the manipulability bounds.

The handle moves in the z-direction in Fig. 11 as commanded, but there is also motion in the y-direction as it approaches the Task 2 singularity just after 3 s. The magnitude of the handle angle-axis rotation vector shown in Fig. 12 should be constant, but error immediately begins to accrue since Task 3 is already in its transition region. The plots of the manipulability indices are shown in Fig. 13. Task 3 reaches its boundary at about 1.7 s, which is when the rotation error in Fig. 12 begins to significantly increase. Task 2 reaches its boundary at about 3.5 s, and the position error begins to accrue in the y-direction. The self-motion angle ϕ remains constant in Fig. 12 as commanded, so Task 4 is evidently unable to help avoid the singularities for the higher priority tasks.

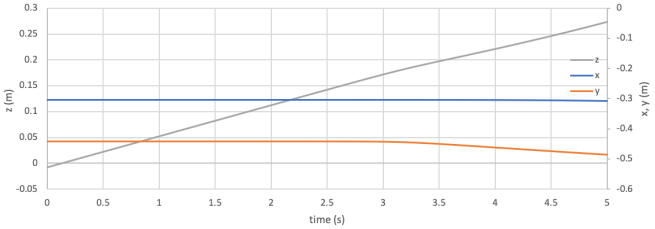

Fig. 11. Handle position during internal singularity trajectory.

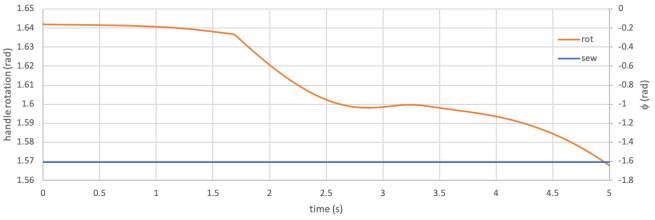

Fig. 12. Magnitude of handle rotation during internal singularity trajectory.

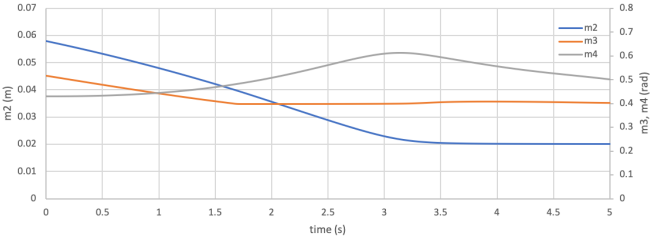

Fig. 13. Manipulability indices for internal singularity trajectory.

VIII. CONCLUSION

A task priority inverse kinematics approach was developed for an 8-axis exoskeleton by partitioning the operational space into four anthropomorphic subtasks. These subtasks were assigned a priority which is used to determine the order in which the inverse kinematics are applied when kinematic constraints are encountered. A task reconstruction approach was used to route the path around singularities so that the exoskeleton can never enter a singular configuration. The application of this approach was demonstrated on the exoskeleton using a robot control computer running the kinematics software on a Linux OS streaming joint angles to a Unity visualization running on a separate computer.

The novelty of the task prioritization approach applied to the exoskeleton is twofold: (a) partitioning of complex inverse kinematics into anthropomorphic subtasks, and (b) evolution of a singularity-free workspace within reach of the operator. This partitioning of the workspace will also enable anthropomorphic application of haptic feedback using feedback from the six-axis force sensors mounted on the upper arm, forearm, and wrist. Future work for the visualization will involve integrating the exoskeleton with other scenes to enable the operator to control the exoskeleton in a mixed reality environment including haptic feedback. This could be used to perform a virtual telerobotic task with haptic feedback while still being able to see the exoskeleton.

APPENDIX

For a robot arm with a three-axis intersecting wrist, the wrist Jacobian can be partitioned as follows

$$J_w = \begin{bmatrix} J_{11} & 0 \\ J_{21} & J_{22} \end{bmatrix} \tag{14}$$

where $J_{11}, J_{21} \in \mathbb{R}^{3\times 4}$ and $J_{22} \in \mathbb{R}^{3\times 3}$ are partitions of the wrist Jacobian, and 0 is a 3×3 matrix of 0's.Using the Cauchy-Binet Formula [11], $J_w J_w^{\mathsf{T}}$ can be transformed into the sum of determinants as follows

$$|J_w J_w^{\mathsf{T}}| = \sum_{i=1}^{4} \left| \begin{pmatrix} J_{11}^i & 0 \\ J_{21}^i & J_{22} \end{pmatrix} \right|^2 + \sum_{i=1}^{3} \left| \begin{pmatrix} J_{11} & 0 \\ J_{21} & J_{22}^i \end{pmatrix} \right|^2 \tag{15}$$

where J_{mn}^i is the i-th submatrix (minor) obtained by suppressing column i of the matrix J_{mn} [20]. The lower block diagonal form of the terms in the first sum in (15) allow it to be reduced to the form

$$\sum_{i=1}^{4} \left| \begin{pmatrix} J_{11}^i & 0 \\ J_{21}^i & J_{22} \end{pmatrix} \right|^2 = |J_{22}|^2 \sum_{i=1}^{4} |J_{11}^i|^2 = |J_{22}|^2 |J_{11} J_{11}^{\mathsf{T}}| \tag{16}$$

The second term in (15) can be expanded into the sum of three minors

$$\sum_{i=1}^{3} \left| \begin{pmatrix} J_{11} & 0 \\ J_{21} & J_{22}^i \end{pmatrix} \right|^2 = M_1^2 + M_2^2 + M_3^2 \tag{17}$$

where M_i is the determinant of J_w with column i+3 suppressed

$$M_i \equiv \left| \begin{pmatrix} J_{11} & 0 \\ J_{21} & J_{22}^i \end{pmatrix} \right| \tag{18}$$

Due to the triangular form of J_w in (14), a sufficient condition for a singular configuration is $rank(J_{11}) < 3$. Since the last three rows of J_w cannot have a rank greater than 3, then $rank(J_w) < 6$ causing $|J_w J_w^{\mathsf{T}}| = 0$. If $rank(J_{11}) = 3$, then $|J_{11} J_{11}^{\mathsf{T}}| \neq 0$ and therefore $|J_{22}| = 0$ in order to make summation in (16) equal to zero. Furthermore, all of the minors in (17) must equal zero, but they only need to be examined for the conditions that cause $|J_{22}| = 0$.

The wrist Jacobian in frame 5 assuming $L_w = 0$ is:

$$J_{11} = \begin{bmatrix} \frac{(L_f + L_u c_5) k_5}{\sqrt{2}} \\ -\frac{L_u k_5 s_5}{\sqrt{2}} \\ (L_f + L_u c_5)(k_4 s_3 + \frac{c_3 s_5}{\sqrt{2}}) - \frac{L_u s_5 (c_3 c_5 - s_3 k_1)}{\sqrt{2}} \end{bmatrix}$$
$$\begin{bmatrix} \frac{(L_f + L_u c_5) c_4}{\sqrt{2}} & \frac{L_f + L_u c_5}{\sqrt{2}} & L_f \\ -\frac{L_u c_4 s_5}{\sqrt{2}} & -\frac{L_u s_5}{\sqrt{2}} & 0 \\ \frac{L_u s_5 k_2}{\sqrt{2}} - (L_f + L_u c_5) k_3 & \frac{L_f s_5}{\sqrt{2}} & 0 \end{bmatrix} \tag{19}$$

$$J_{21} = \begin{bmatrix} -s_3 k_4 - \frac{c_3 s_5}{\sqrt{2}} & k_3 & -\frac{s_5}{\sqrt{2}} & 0 \\ \frac{s_3 k_1 - c_3 c_5}{\sqrt{2}} & \frac{k_2}{\sqrt{2}} & -\frac{c_5}{\sqrt{2}} & 0 \\ \frac{k_5}{\sqrt{2}} & \frac{c_4}{\sqrt{2}} & \frac{1}{\sqrt{2}} & 1 \end{bmatrix} \tag{20}$$

$$J_{22} = \begin{bmatrix} 0 & s_6 & c_6 s_7 \\ -1 & 0 & c_7 \\ 0 & -c_6 & s_6 s_7 \end{bmatrix} \tag{21}$$

where $c_i \equiv \cos(\theta_i)$, $s_i \equiv \sin(\theta_i)$, and the k_i are defined as

$$k_1 \equiv s_4 c_5 + \sqrt{2} c_4 s_5 \tag{22}$$
$$k_2 \equiv c_4 c_5 - \sqrt{2} s_4 s_5 \tag{23}$$
$$k_3 \equiv s_4 c_5 + c_4 s_5 / \sqrt{2} \tag{24}$$
$$k_4 \equiv c_4 c_5 - s_4 s_5 / \sqrt{2} \tag{25}$$
$$k_5 \equiv c_3 + s_3 s_4 \tag{26}$$

The determinants of J_{11} with column j suppressed, J_{11}^j, are given by

$$|J_{11}^1| = -\frac{L_f L_u}{\sqrt{2}} s_5 (L_u s_4 + L_f k_1) \tag{27}$$
$$|J_{11}^2| = \frac{L_f L_u}{\sqrt{2}} s_3 s_5 (L_u c_4 + L_f k_2) \tag{28}$$
$$|J_{11}^3| = \frac{L_f L_u}{\sqrt{2}} s_5 [(L_u + L_f c_5) s_3 + (L_u s_4 + L_f k_1) c_3] \tag{29}$$
$$|J_{11}^4| = 0 \tag{30}$$

The determinant of J_{22} is given by $|J_{22}| = s_7$. The minors of the wrist Jacobian ${}^5J_w^j$ are given by

$$M_5|_{s_7=0} = M_7|_{s_7=0} = L_f L_u^2 s_3 c_6 s_5^2 \tag{31}$$
$$M_6|_{s_7=0} = 0 \tag{32}$$

ACKNOWLEDGMENT

This project was sponsored by the NASA Exploration and In-Space Services (NEXIS) Projects Division at NASA Goddard Space Flight Center under OMES Contract #NNG12CR31C.

REFERENCES

[1] J. Andrews and Y. Youm, "A biomedical investigation of wrist kinematics," *Journal of Biomechanics*, vol. 12, pp. 83–93, 1979.

[2] P. Baerlocher and R. Boulic, "Task-priority formulations for the kinematic control of highly redundant articulated structures," in *Proc. IEEE/RSJ International Conference on Intelligent Robots and Systems*, Victoria, BC, Canada, Oct. 1998, pp. 323–329.

[3] F. Caccavale, S. Chiaverini, and B. Siciliano, "Second-order kinematic control of robot manipulators with jacobian damped least-squares inverse: Theory and experiments," *IEEE/ASME Transactions on Mechatronics*, vol. 2, no. 3, pp. 188–194, Sept. 1997.

[4] C. Carignan, J. Tang, and S. Roderick, "Development of an exoskeleton haptic interface for virtual task training," in *Proc. IEEE/RSJ International Conference on Intelligent Robots and Systems*, St. Louis, Oct. 2009, pp. 3696–3702.

[5] C. Carignan, J. Tang, S. Roderick, and M. Naylor, "A configuration-space approach to controlling a rehabilitation arm exoskeleton," in *Int. Conf. on Rehabilitation Robotics (ICORR)*, Noordwijk, Netherlands, June 2007, pp. 179–187.

[6] K.-S. Chang and O. Khatib, "Manipulator control at kinematic singularities: A dynamically consistent strategy," in *International Conference on Intelligent Robots and Systems*, vol. 3, Pittsburgh, PA, Aug. 1995, pp. 3084–3088.

[7] S. Chiaverini, "Singularity-robust task-priority redundancy resolution for real-time kinematic control of robot manipulators," *IEEE Transactions on Robotics and Automation*, vol. 13, no. 3, pp. 398–410, June 1997.

[8] S. Chiaverini, B. Siciliano, and O. Egeland, "Review of the damped least-squares inverse kinematics with experiments on an industrial robot manipulator," *IEEE Transactions on Control Systems Technology*, vol. 2, no. 2, pp. 123–134, June 1994.

[9] J. Craig, *Introduction to Robotics: Mechanics and Control, 2nd ed.* Reading, Mass.: Addison-Wesley, 1989.

[10] Z. Cui, H. Pan, D. Qian, Y. Peng, and Z. Han, "A novel inverse kinematics solution for a 7-DOF humanoid manipulator," in *Proc. IEEE International Conference on Mechatronics and Automation*, Chengdu, China, Aug. 2012, pp. 2230–2234.

[11] F. R. Gantmacher, *The Theory of Matrices, Vol. I.* Providence, Rhode Island: American Mathematical Society, 1989.

[12] M. Hessinger, M. Pingsmann, J. Perry, R. Werthschützky, and M. Kupnik, "Hybrid position/force control of an upper-limb exoskeleton for assisted drilling," in *Proc. IEEE/RSJ International Conference on Intelligent Robots and Systems*, Vancouver, BC, Canada, Sept. 2017, pp. 1824–1829.

[13] T. James and C. Carignan, "Exoskeleton wrist design using composite visualization methods," in *ASME International Mechanical Engineering Congress and Exposition (IMECE)*, Phoenix, Nov. 2016.

[14] G. R. Johnson, D. A. Carus, G. Parrini, S. S. Marchese, and R. Valeggi, "The design of a five-degree-of-freedom powered orthosis for the upper limb," in *Proc. Instn. Mech. Engrs. Part H*, vol. 215, 2001, pp. 275–284.

[15] A. Q. L. Keemink, G. van Oort, M. Wessels, and A. H. A. Stienen, "Differential inverse kinematics of a redundant 4r exoskeleton shoulder joint," *IEEE Transactions on Neural Systems and Rehabilitation Engineering*, vol. 26, no. 4, pp. 817–829, Apr. 2018.

[16] H. Kim, L. M. Miller, N. Byl, G. M. Abrams, and J. Rosen, "Redundancy resolution of the human arm and an upper limb exoskeleton," *IEEE Transactions on Biomedical Engineering*, vol. 59, no. 6, pp. 1770–1779, June 2012.

[17] J. Kim, G. Marani, W. K. Chung, and J. Yuh, "Dynamic task priority approach to avoid kinematic singularity for autonomous manipulation," in *IEEE/RSJ International Conference on Intelligent Robots and Systems*, Lausanne, Switzerland, Oct. 2002, pp. 1942–1947.

[18] J. Kim, G. Marani, W. K. Chung, J. Yuh, and S.-R. Oh, "A general singularity avoidance framework for robot manipulators: Task reconstruction method," in *IEEE International Conference on Robotics and Automation*, New Orleans, Apr. 2004, pp. 4809–4814.

[19] N. Klopcar and J. Lenarcic, "Kinematic model for determination of human arm reachable workspace," *Meccanica*, vol. 40, pp. 203–219, 2005.

[20] R. Konietschke, G. Hirzinger, and Y. Yan, "All singularities of the 9-dof dlr medical robot setup for minimally invasive applications," in *Advances in Robot Kinematics: Mechanisms and Motion*, Ljubljana, Slovenia, Jan. 2006, pp. 193–200.

[21] K. Kreutz-Delgado, M. Long, and H. Seraji, "Kinematic analysis of 7 DOF manipulators," *Int. Journal of Robotics Research*, vol. 11, no. 5, pp. 469–481, 1992.

[22] M. Liszka, "Mechanical design of a robotic arm exoskeleton for shoulder rehabilitation," Master's thesis, University of Maryland, Dec 2006.

[23] G. Marani, J. Kim, J. Yuh, and W. K. Chung, "Algorithmic singularities avoidance in task-priority based controller for redundant manipulators," in *Proceedings of the IEEE/RSJ International Conference on Intelligent Robots and Systems*, Las Vegas, 2003, pp. 3570–3574.

[24] T. B. Moeslund, C. B. Madsen, and E. Granum, "Modelling the 3D pose of a human arm and the shoulder complex utilising only two parameters," in *Proc. of the Intl. Conference on Model-based Imaging, Rendering, Image Analysis and Graphical Special Effects*, INRIA Rocquencourt, France, 2003, pp. 11–19.

[25] Y. Nakamura, *Advanced Robotics: Redundancy and Optimization*. Addison Wesley, 1991.

[26] Y. Nakamura and H. Hanafusa, "Inverse kinematic solutions with singularity robustness for robot manipulator control," *Journal of Dynamic Systems, Measurement, and Control*, vol. 108, no. 3, pp. 163–171, Sept. 1986.

[27] A. Schiele and F. C. T. van der Helm, "Kinematic design to improve ergonomics in human machine interaction," *IEEE Transactions on Neural Systems and Rehabilitation Engineering*, vol. 14, no. 4, pp. 456–469, Dec. 2006.

[28] L. Sciavicco and B. Siciliano, *Modeling and Control of Robot Manipulators, 2nd Ed.* London: Springer-Verlag, 2000.

[29] C. W. Wampler, "Manipulator inverse kinematic solutions based on vector formulations and damped least-squares methods," *IEEE Transactions on Systems, Man, and Cybernetics*, vol. SMC-16, no. 1, pp. 93–101, Jan. 1986.

[30] T. Yoshikawa, "Manipulability of robotic mechanisms," *International Journal of Robotics Research*, vol. 4, no. 2, pp. 3–9, 1985.